Nucleic Acids Research, 2025, **53**, gkaf1052
https://doi.org/10.1093/nar/gkaf1052
Chemical Biology and Nucleic Acid Chemistry

Affinity-selected peptide ligands specifically bind i-motif DNA and modulate c-Myc gene expression

Dilek Guneri [1], Summer Rosonovski [2], Effrosyni Alexandrou [1], Shuang Chen [1], Jessica King [3], Christopher A. Waudby [1], Shozeb Haider [1,4,5], Christoper J. Morris [1,*], Zoë A.E. Waller [1,*]

[1]UCL School of Pharmacy, 29-39 Brunswick Square, London WC1N 1AX, United Kingdom
[2]School of Pharmacy, University of East Anglia, Norwich Research Park, Norwich NR4 7TJ, United Kingdom
[3]School of Molecular Sciences, University of Western Australia, Crawley, Western Australia 6009, Australia
[4]University of Tabuk (PFSCBR), Tabuk 71491, Saudi Arabia
[5]UCL Centre for Advanced Research Computing, University College London, WC1H 9RN, United Kingdom

*To whom correspondence should be addressed. Email: z.waller@ucl.ac.uk
Correspondence may also be addressed to Christopher Morris. Email: chris.morris@ucl.ac.uk

Abstract

c-Myc is an oncogene that is dysregulated in ~70% of cancers. Its multifaceted function complicates effective drug targeting of the protein. i-Motif (iM) DNA structures in gene promoter regions have gained attention for their potential role in the modulation of gene expression. These include the iM formed by the cytosine-rich sequence which lies upstream of the key P1 promoter of the c-Myc gene. Currently, selective ligands interacting with iM structures are limited. Here, peptide ligands for the iM from the promoter of c-Myc were identified via phage display. Hit peptides were filtered for selective binding to iM structures over other DNA structures using displacement assays and DNA melting experiments. Two lead peptides were found to produce dose-dependent changes in c-Myc gene expression after delivery into HEK293 cells expressing a c-Myc luciferase reporter construct. These leads may be used as chemical tools for the manipulation of c-Myc iM *in vitro* and have the potential to be developed into cell-permeable peptidomimetics for delivery *in vivo*.

Graphical abstract

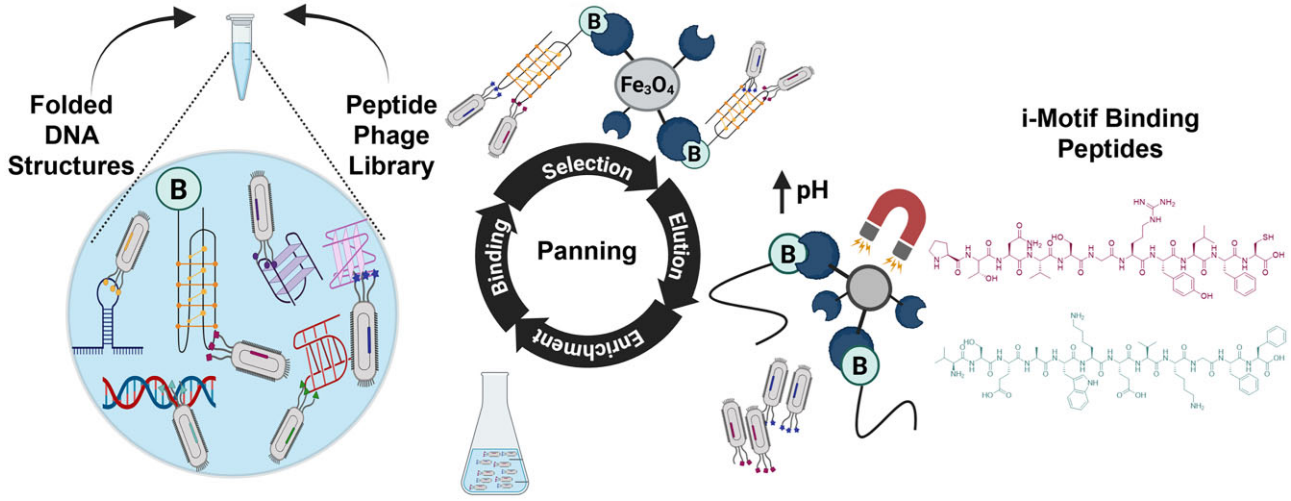

Introduction

The proto-oncogene, c-Myc, is a multifunctional transcription factor which controls various downstream genes and coordinates a range of cellular processes in both health and disease [1]. Elevated expression of c-Myc in cancer occurs through several mechanisms (e.g. gene amplification and chromosomal translocation) and results in elevated tumour aggression and poorer clinical outcomes [2]. Substantial experimental evidence has established that reducing overactive c-Myc can lead to cancer regression [1, 3–5]. One approach to direct targeting of the Myc protein is achieved by interference with the Myc-Max heterodimerization. The peptide/protein candidates, OMO-103 and IDP-121, have progressed to Phase I clinical testing. OMO-103 dose-escalation trial results indicate that this is a tractable approach that can deliver anti-tumour activity across different tumor types [6].

Received: December 5, 2024. **Revised:** September 22, 2025. **Accepted:** September 23, 2025

A significant challenge for all protein/peptide-based drugs is the requirement to deliver an intracellular dose that is sufficient to neutralize all copies of the c-Myc protein in a cancer cell. These have been estimated to number 30 000 copies per cell [7]. Reports of siRNA-mediated knockdown of c-Myc mRNA levels indicate that this approach has merit, yet efficient intracellular delivery of small interfering RNA (siRNA) can be similarly challenging and inefficient. A contrasting and arguably more potent approach involves targeting the c-Myc gene directly, such that MYC levels are suppressed pretranscriptionally through blockade of key protein–DNA promoter interactions. This approach is particularly appropriate considering the short half-life of both c-Myc mRNA (10 min) and protein (20 min) [8].

c-Myc transcription is largely controlled by the P1 and P2 promoter sites [9]. Upstream of the P1 promoter regulatory region, there is a nuclease hypersensitivity element (NHE)-III_1 that is prerequisite for ∼90% of c-Myc gene transcription [10–12]. This element contains guanine-cytosine (GC)-rich sequences capable of forming non-canonical DNA structures: i-motifs (iMs) and G-quadruplexes (G4s). iMs are formed from cytosine-rich sequences, zipped together through hemiprotonated cytosine–cytosine base pairs [13, 14], whereas G4s on the opposing strand form in guanine-rich sequences, stabilized by Hoogsteen hydrogen bonding and physiologically relevant cations [15]. G4-formation within the NHE III_1 region has been extensively studied, showing that destabilizing G4 structure leads to increased c-Myc transcription and stabilizing the G4 represses transcription [16–18]. c-Myc transcription is proposed to be initiated by the negative supercoiling of the NHE-III_1 region which facilitates the G4 formation and creates a transient single-stranded region recognizable for elements of the transcription machinery. This may include helicases able to resolve the G4 structure and promote c-Myc expression [19]. However, negative supercoiling alone may not be the key mechanism to facilitate G4 formation [20]. Further insights into the regulatory region of the c-Myc promoter region are required to facilitate the development of novel ligands and potential drugs. This includes exploration and study of the potential of iM-formation on the opposing strand [21]. iM-forming sequences are well-characterized to be able to form *in vitro* at neutral pH [22, 23] and have been shown to be present and involved in transcription and proliferation in cells [24–26]. More recently, there have been reports of iM-binding small molecules [27], but selectivity remains an issue for iM ligands. Indeed, even many G4-binding ligands have also been found to interact with diverse iM structures [28, 29]. Consequently, the discovery of specific iM-binding ligands is crucial to develop both target-specific chemical tools and future therapeutics, both for c-Myc and other iM-forming regions in the genome.

Specific nucleoproteins have been found to bind both iMs or G4 structures and subsequently modulate gene expression levels. Heterogeneous nuclear ribonucleoprotein K (hnRNP-K) is an RNA/DNA-binding protein that binds to single-stranded, cytosine-rich sequences. It was shown by Hurley *et al.* to bind and unfold the iM-forming sequence of c-Myc and to increase c-Myc transcription [30]. This was indirectly validated by others who observed that hnRNP-K gene-knockdown reduced MYC protein levels [31]. More recent work has demonstrated different ways to target specific DNA G4s, including c-Myc, using CRISPR-Cas9 guided G4-binding proteins and ligands [32, 33]. Drawing inspiration from the binding activity of nucleoproteins, we aimed to identify peptidic ligands that could regulate quadruplex biology. Unlike non-selective small molecules and large antibody species, these peptide ligands would occupy a molecular size niche with potential for increased specificity compared to small molecules and improved intracellular delivery capabilities compared to antibodies. Here, we deployed phage display to select peptide ligands that bind selectively to the iM-structure in the c-Myc promoter.

Materials and methods

Chemicals were purchased from Sigma–Aldrich/Merck, were of analytical or molecular biology grade, and used without further purification.

Oligonucleotides (listed in Supplementary Tables S1 and S2) were purchased from Eurogentec and were RP-HPLC purified. Solid DNA samples were initially dissolved in ultrapure water to a concentration of 1 mM. Stock concentrations were confirmed using the extinction coefficients provided by Eurogentec, and their UV absorbance at 260 nm was determined with a Nanodrop ND-1000 spectrophotometer. The samples were prepared as 10 μM DNA in 10 mM sodium cacodylate (NaCaco) buffer at the specified pH and thermally denatured at 95°C for 5 min and allowed to anneal slowly to room temperature overnight. pH 6.6 was used for most of the biophysical studies as it is the transitional pH of c-Myc, the pH where 50% of the sequence is folded into iM [30].

Phage display of peptides and c-Myc i-motif ligand selection

The NEB Ph.D.™-12 library, containing ∼10^9 randomized, linear peptide sequences was panned against c-MycC52 iM following the protocol described in the NEB Phage Display instruction manual. Key buffers used in the library panning were as follows: incubation buffer (PBS pH 6.0), wash buffer (PBS, pH 6.0 with 0.01%–0.05% Tween 20), blocking buffer (PBS, pH 6.0 with 5 mg/ml bovine serum albumin (BSA)), and elution buffer (phosphate-buffered saline (PBS), pH 7.4) (Supplementary Table S3). Phage display library panning involved solution-phase panning with a 5′-biotinylated c-MycC52 target and target capture on High-Capacity Streptavidin coated plates. PBS was the DNA buffer of choice for phage display as it has a good buffering range across pH 5.8–7.4. c-MycC52 is unfolded at pH 7.4, fully folded at pH 5.8, and 50% folded at pH 6.44 (Supplementary Fig. S1), consistent with previous reports by Hurley *et al.*[30]. PBS (pH 6.0) was chosen as the incubation buffer, as this is slightly more acidic than the transitional pH of c-MycC52 in PBS (Supplementary Fig. S1). Supplementary Table S3 summarizes the three rounds of phage display screening that were undertaken. The target c-MycC52 oligonucleotide was used alone in round one. Unbiotinylated competitor oligonucleotides were used in rounds two and three at the concentrations indicated in Supplementary Table S3. At the end of each screening round, phages were enumerated by titration with *Escherichia coli* ER2738 and amplified in *E. coli* ER2738 as per NEB's phage display manual. At the end of round three, 25 individual phage plaques were harvested from IPTG/X-Gal plates and amplified on a 5 ml scale for 4 h. Single stranded phage DNA was isolated after iodide denaturation and ethanol precipitation. DNA was sequenced

using Sanger sequencing (Mix2Seq Eurofins) using the -96 gIII sequencing primer provided by NEB.

Peptides were purchased from Cellmano Biotech (Hefei, China) as RP-HPLC-purified (>95%) with N-terminal acetylation and C-terminal amidation to mimic the phage-displayed fusion peptides. Stock solutions of the peptides were made at 5 mg/ml in ultrapure water or dimethyl sulfoxide (DMSO) (if water insoluble) and were stored at −20°C. Subsequent dilutions were made in the appropriate assay buffer. Stock concentrations were confirmed using the peptide extinction coefficients and UV absorbance on an Agilent Technologies Cary 4000 UV–VIS spectrometer. The Nick Anthis Protein Parameter Calculator was used to determine the extinction coefficient either at 280 nm if the sequence contained any tryptophan or tyrosine residues or at 205 nm if the sequence contained neither of these amino acids [34].

Fluorescent indicator displacement (FID) experiments used in this publication are based on the first FID assay developed for iM DNA [35]. The FID experiments were performed on a BMG CLARIOstar plate reader using 96-well, solid black flat-bottom plates. Thiazole Orange (TO) was the indicator, and the stock solution was prepared at 10 mM in DMSO. The TO stock was diluted into the appropriate buffer to 2 μM. Each well received 9 μl of the 2 μM TO solution, was excited at 430 nm, and fluorescence emission at 450 nm was measured; this was normalized to 0% to account for background fluorescence. One microlitre of 90 μM DNA was added to each well and shaken in the plate reader for 30 s using double orbital shaking at 700 rpm and left for 10 min to equilibrate. Following equilibration, fluorescence emission was measured and normalized to 100% representing maximum fluorescence. Peptides were titrated starting at 25 μM, with 0.9 μl additions into each well in triplicate, until a final concentration of 200 μM was reached, and fluorescence emission was measured after each addition. Fluorescence emission for each well was normalized between 0% and 100%, which was taken away from 100 to give the percentage of displacement. The data were analyzed in Origin data analysis software and fitted with a hyperbolic dose–response curve from which the DC_{50} value was interpolated.

Circular Dichroism (CD) melting experiments were performed in a Jasco J-1500 spectropolarimeter with 10 μM DNA samples in 10 mM sodium cacodylate buffer at pH 6.6 using a 1 mm path length quartz cuvette. Initially, two repeats of CD melting full spectrum ranges were taken (from 230 to 320 nm) for c-MycC27, c-MycC52, c-MycG27, c-MycG52, and double-stranded DNA (dsDNA) (Supplementary Table S1), measuring the unfolding of the DNA structures from 5°C to 95°C in the presence of 10 molar equivalent DMSO, Pep-PTN, or Pep-VSE as well as Pep-SLC and buffer for dsDNA. The samples were kept at 5°C for 5 min before starting the melt, with a temperature increase of 1°C/min, a 0.5°C data interval, and a 60-s holding time at each target temperature. Four scans were accumulated data pitch of 0.5 nm, a scanning speed of 200 nm/min, 1 s response time, 2 nm bandwidth, and 200 mdeg sensitivity. Furthermore, two CD melting experiment repeats were performed recording C-rich c-Myc at 288 and 320 nm, G-rich c-Myc at 264 and 320 nm, and dsDNA at 253 and 320 nm with the settings as described for full spectrum measurements. Data were zero corrected to 320 nm and baseline drift. The melting temperature (T_M) was concluded using the Boltzmann or biphasic fitting curve on the folded fraction data using GraphPad Prism version 10.1.2. Data were processed as mean ± SEM ($n = 4$) and one-way ANOVA followed by Bonferroni post-hoc test to determine significant changes between peptides and controls.

UV titrations were recorded using an Agilent Cary-60 UV/VIS spectrometer with a 10 mm path length black-walled quartz cuvette. Oligonucleotides (c-MycC27, c-MycC52, c-MycG27, c-MycG52, DAPc, DAPg, and dsDNA; sequences listed in Supplementary Table S1) were annealed as 250 μM stock solutions in 10 mM sodium cacodylate buffer (pH 6.6) in the presence or absence of 100 mM KCl. Spectra were recorded at room temperature over a wavelength range of 300–500 nm with 1 nm intervals. Buffer-only spectra were recorded and subtracted from each dataset as blanks. Peptide ligands were prepared as 1 mM stock solutions in DMSO and added to the cuvette at a final concentration of 10 μM in buffer prior to DNA addition. DNA stock was diluted to 50 μM in buffer and was added stepwise to the peptide solution to reach 2.5 μM final concentration, followed by additions from the 250 μM DNA stock to reach final DNA concentrations of 30 or 50 μM. The absorbance at 350 nm was monitored and plotted against DNA concentration. Binding curves were fitted using a one-site binding model in GraphPad Prism version 10.1.2, and K_d values were determined from normalized data to represent the DNA-ligand bound fraction.

NMR: ^{1}H NMR spectra of c-MycC52 were recorded at 283 K using a Bruker Avance NEO 600 MHz spectrometer equipped with QCI-F cryoprobe operating Topspin 4.5.0. Spectra were recorded with excitation sculpting, at 27.75 ppm spectral width, 1 s acquisition time, and 1 s recycle delay. Spectra of the imino proton region were acquired with a 1D SOFAST excitation scheme with a 1293 μs Pc9_4_120 excitation pulse and 720 μs Reburp refocusing pulse, centred at 13 ppm, a 29.75 ppm spectral width, 115 ms acquisition time, and 100 ms recycle delay. Samples were annealed at a final concentration of 50 μM in 10 mM sodium cacodylate (pH 6.6). 10% D_2O and 0.01% sodium trimethylsilylpropanesulfonate (DSS) were added immediately before recording NMR spectra experiments. Spectra were processed with exponential line broadening and referenced to the Sodium trimethylsilylpropanesulfonate (DSS) chemical shift. The chemical shift of the cacodylate buffer resonance was used to monitor potential pH changes between samples.

Cell studies: HEK293 cells (ATCC CRL-1573™, passages 20–28), MCF-7 cells (ATCC HTB-22™, passages 21–28), and Panc-1 cells (ATCC CRL-1469™, passages 15–22) were cultured in Dulbecco's Modified Eagle's Medium (DMEM) medium supplemented with 10% fetal bovine serum (FBS; Gibco, UK) and maintained under standard cell culture conditions (37°C, 5% CO_2). Cells were passaged every 3–4 days at ∼80% confluency. For experiments, the cells were seeded into six-well plates at a density of 1×10^5 cells/well in DMEM containing 10% FBS. At ∼80% confluency, HEK293 wild-type cells were co-transfected with the c-Myc promoter (Del-4) Firefly luciferase plasmid [36] (a gift from Bert Vogelstein; Addgene plasmid #16 604; http://n2t.net/addgene:16604;RRID:Addgene_16 604) and a control Renilla luciferase reporter vector (Promega, pRL-TK Vector; GenBank® Accession Number AF025846) at a 3:1 plasmid ratio. In parallel, the pGL410_INS421 plasmid [37] (a gift from Kevin Ferreri; Addgene plasmid #49 057; http://n2t.net/addgene:49057;RRID:Addgene_49 057), which contains the human insulin promoter with 2.5 insulin-linked polymorphic region (ILPR) repeats regulating firefly luciferase expression [38], was trans-

fected as a control for promoter activation. Plasmid DNA and Lipofectamine™ 2000 (Invitrogen, UK) were mixed at a 1:1 ratio and incubated at room temperature for 15 min before transfecting HEK293 cells. The following day, HEK293 transfected with reporter vectors for c-Myc or ILPR were reseeded into white and transparent 96-well plates (Greiner Bio-One, Germany) at a density of 5×10^4 cells/well in DMEM containing 2% FBS. Cells were treated in duplicates with 1, 5, or 10 μM of Pep-PTN or Pep-VSE, or with 0.2% DMSO as a vehicle control, in the presence or absence of Nanocin PRO (Tecrea, UK) as a peptide delivery reagent. In addition, HEK293 wild-type, MCF-7 cells, and Panc-1 cells were also seeded at 5×10^4 cells/well into transparent 96-well plates in DMEM with 2% FBS for cell proliferation assays. Cell proliferation was assessed at 4 and 24 h post-treatment using the CellTiter 96® Aqueous One Solution Cell Proliferation Assay (Promega, USA). For this, 20 μl of reagent was added per well, and absorbance at 490 nm was measured after 4 and 24 h using a SpectraMax iD3 plate reader (Molecular Devices, UK). Blank values (media without cells) were subtracted, and readings were normalized to DMSO-treated controls. In parallel, Dual-Luciferase Reporter Assays (Promega, USA) were performed in white 96-well plates to determine promoter activation regulated by c-Myc or ILPR promoter regions. Firefly luciferase signals were normalized to Renilla luciferase signals and further normalized to the 0.2% DMSO control condition. All data represent the mean ± standard deviation (SD) from six to eight biological replicates. Statistical significance was determined using one-way ANOVA followed by Holm–Šídák post-hoc analysis performed in GraphPad Prism version 10.1.2.

Computational studies

A model of the c-Myc iM with a sequence of 41 nucleotides was built (5′-CTTCTCCCCACCTTCCCCACCCTCCCCACCCTCCCCATAAG-3′). This model was based on the intramolecular iM structure from the ILPR [38] and folding conformations proposed by Sutherland *et al.* [30] (Supplementary Fig. S21). Adaptive bandit enhanced sampling molecular dynamics simulations [38, 39] were employed to sample the loop and flank conformations of this model. Markov state models were then built to cluster metastable states using the PyEMMA package [40]. From these, the two most stable states were chosen to carry out molecular docking with the PTN and VSE peptides. *De novo* 3D structure predictions for these peptides were performed, using the PEP-FOLD3 web server (https://bioserv.rpbs.univ-paris-diderot.fr/services/PEP-FOLD3/). Docking was subsequently performed using the HDOCK web server (http://hdock.phys.hust.edu.cn/). Full details of all the protocols are listed in the Supplementary Information.

Results and discussion

Phage display is a recombinant screening technique that permits the rapid screening of libraries with diversity up to 10^9 unique ligand peptides or antibody fragments against a given target, such as iM and G4 structures [24, 41]. We screened a linear peptide library (NEB Ph.D™.-12) against the biotinylated 52 bp C-rich c-Myc promoter sequence (c-MycC52, 5′-CTT-CTC-CCC-ACC-TTC-CCC-ACC-CTC-CCC-ACC-CTC-CCC-ATA-AGC-GCC-CCT-CCC-G-3′).

Table 1. Peptide sequences determined from three rounds of panning of Phage Display against c MycC52 using the NEB Ph.D™.-12 linear randomized library

Peptide ligand	Amino acid sequence
Pep-EIE	EIEY**TDHMK**ELG
Pep-PTN	PTNVSGRNYLFC
Pep-RVS	RVS**TDHMK**GRGG
Pep-SLC	SLCDIIRIEKVR
Pep-VSE	VSEAWKEVKGFF

Conserved sequence shown in bold; consensus sequence underlined.

This longer-length c-Myc sequence has been shown to be necessary for effective transcriptional firing from the P1 and P2 promoters [30, 42]. The selection pressure for each round of panning was increased by reducing the amount of biotinylated target c-MycC52 used and adding non-biotinylated competitor DNA sequences. Round one of panning used 10 pmol. of c-MycC52 alone, without competitors. Rounds two and three reduced the amount of c-MycC52 target and then added non-biotinylated competitors. Competitors included in round two included three different types of G4s, a short double-stranded sequence, a Holliday junction, single-stranded RNA, a C-rich hairpin which does not form iM, and calf-thymus DNA. Round three had a range of competing iM-forming sequences which represent a range of C-stack and loop lengths, with varying pH stabilities: sequences from the human telomere, the ILPR, and the promoter regions of ATXN2L, DAP, and Hif1α (Supplementary Tables S2 and S3). DNA sequencing was performed at the end of round three to determine the sequence of the selected peptides, which revealed a total of five different peptides (Table 1). Full sequences, structures, and purity of the peptides purchased and subsequently used are provided in Supplementary Table S4.

The most enriched peptide was Pep-EIE, which shared a TDHMK motif with Pep-RVS. Three peptides contained the consensus sequence: (S/T)(D/E)XX^2X^3, where X is any amino acid, X^2 is a large amino acid, and X^3 is a basic amino acid. Pep-SLC included the closely related sequence, DIIR. Pep-PTN and Pep-SLC both included at least one arginine residue, which are typically depleted in the particular phage display library used [43]. Conventionally, arginine residues favour binding to pyrimidine-rich DNA regions, as evidenced by the abrogated binding of NM23-H2 to single-stranded DNA after the substitution of a key arginine for alanine, reducing interactions with the phosphodiester backbone [44].

The relative binding of the five peptide ligands to the folded c-MycC52 iM was assessed via a FID assay [30] using TO (Fig. 1). These experiments were performed in 10 mM sodium cacodylate at pH 6.6, the transitional pH of the c-Myc iM-forming sequence. As iM-formation is reduced at higher pH and higher ionic strength [45], additional stabilizing cations were avoided to allow the highest proportion of iM formation at the highest pH, to represent as close to physiological pH conditions as possible.

All five peptides demonstrated concentration-dependent intercalator displacement from the c-MycC52 iM. The relative binding affinity was ranked as SLC > PTN > VSE > EIE > RVS. All were able to show displacement of TO from the c-MycC52 sequence, with average displacement values at 100 μM spanning 5%–85%. It is important to note that the TO assay gives an indication of displacement, rather than direct binding. Accepting that this method only determines which

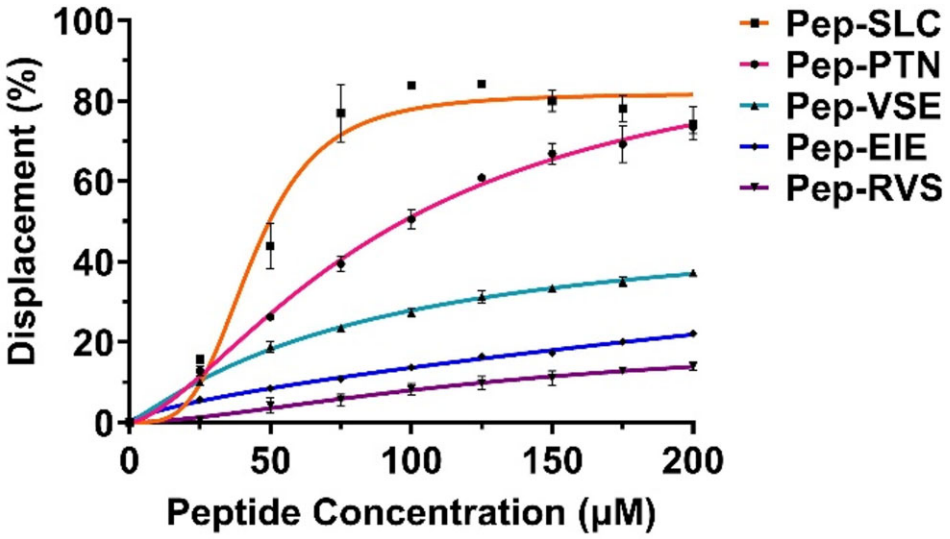

Figure 1. Concentration-dependent interaction of peptides with c-MycC52 iM determined via FID assay. The assay was performed with 1 μM c-MycC52 in 10 mM sodium cacodylate, pH 6.6, in the presence of 2 μM TO. Peptide ligands were added in increments of 25 μM up to a final concentration of 200 μM. Data are presented as mean ± SD ($n = 3$) and fitted using a Hill-Slope dose–response curve.

peptides displace the TO, and that the peptides may also bind other sites on this extended iM, we took the top three peptides SLC, PTN, and VSE forward for further study at this stage.

To determine the effects of peptide binding on iM stability, we measured DNA melting points (T_M) using CD-based melting experiments. The three remaining peptides were initially tested for off-target binding to dsDNA. Pep-SLC destabilized dsDNA by 5°C (Supplementary Figs S2A and S3). Pep-PTN and Pep-VSE had no effect on dsDNA melting compared to the solvent controls (Supplementary Figs S2B and S4). As we were interested in characterizing peptides with the maximum specificity, we elected to exclude Pep-SLC from further characterization at this time, though this peptide may still have utility for targeting c-Myc. We tested the thermal stability of c-MycC52 iM and a shorter analogue c-MycC27 (5′-CCT-TCC-CCA-CCC-TCC-CCA-CCC-TCC-CCA-3′) (Supplementary Fig. S5) as well as their complementary G4-forming sequences (c-MycG52 5′-CGG-GAG-GGG-CGC-TTA-TGG-GGA-GGG-TGG-GGA-GGG-TGG-GGA-AGG-TGG-GGA-GAA-G-3′) and c-MycG27 (5′-TGG-GGA-GGG-TGG-GGA-GGG-TGG-GGA-AGG-3′), respectively, in Supplementary Fig. S6, in the presence of 10 molar equivalents of Pep-PTN or Pep-VSE. The stabilization temperatures are summarized in Supplementary Table S5, and full melting curves are shown in Supplementary Figs S2–S4 and S7–S10. Both c-MycC27 and c-MycC52 sequences exhibited a double transition in the CD melts, implying two folded populations with different stabilities (Supplementary Fig. S5). This was not unexpected, as both sequences have the capabilities of folding into different structures because of their length [41]. We determined the T_Ms of both species due to the likely existence of both iM topologies *in vivo*. The c-MycC27 and c-MycG27 sequences were neither stabilized nor destabilized by Pep-PTN nor PEP-VSE (Table 2, and Supplementary Figs S5B and S7B). In contrast, the peptides significantly modulated the thermal stability of the biologically relevant c-MycC52 and the complementary G-rich sequence ($P < 0.001$***). Specifically, both iM populations formed by c-MycC52 showed significant destabilization in the presence of Pep-VSE (Table 2 and Supplementary Fig. S5A). Interestingly, the T_M decrease of the c-MycC52 sequence was greater for the more stable iM population, with a ΔT_M of -14 ± 0.5°C ($P < 0.001$***, see Supplementary Fig. S5A).

In contrast, Pep-PTN caused a modest, 2 ± 0.3°C decrease in T_M ($P < 0.05$) of the more stable iM population with no significant change to lower T_M value. The complementary c-MycG52 sequence was modestly stabilized by both Pep-PTN (+2°C, $P < 0.05$) and Pep-VSE (+4°C, $P < 0.01$**) (Table 2 and Supplementary Fig. S6A). To the best of our knowledge, these are the first examples of ligands to target the long c-MycC sequence. There are a few ligands that have been found to target shorter versions of the sequence. For example, Shu *et al.* developed compound B19 which was found to stabilize the shorter c-MycC27 sequence (ΔT_M: 11.5°C) [46]. Saha *et al.* found a compound that stabilized a 33-mer variant of c-Myc (ΔT_M: 29.7°C) [47], and Debnath *et al.* found a compound that stabilized the same sequence with a ΔT_M value of 32°C [48]. Di Porzio *et al.* [49] examined compounds against a 22-mer version and their best compound against that sequence of c-Myc showed a ΔT_M of −27.5°C.

To support the experiments on the stabilizing properties of the peptides, we also performed direct binding measurements of Pep-VSE and Pep-PTN using UV titrations. Binding curves are provided in Supplementary Fig. S11, and K_ds are in Table 2. These experiments reveal tight binding of both PTN (0.93 ± 0.08 μM) and VSE (0.43 ± 0.03 μM) compared to other DNA structures. Although binding was detected for both peptides against c-MycG52, the G4-forming sequence in the complementary strand, there was no plateau at the concentrations examined. So, we have estimated a lower limit of 50 μM as the potential dissociation constant. Binding measurement against the iM- and G4-forming sequence from the promoter region of death-associated protein (DAPc and DAPg, respectively) and dsDNA showed no concentration-dependent or saturable binding event to either peptides, indicating non-specific binding under the tested conditions. As much of the work we performed with c-MycC52 was done in the absence of additional stabilizing monovalent cations, to enable exper-

Table 2. Destabilization and binding properties of Pep-PTN and Pep-VSE. *CD melting analysis of 10 μM c-MycC27 and c-MycC52 and their complementary c-MycG sequences in 10 mM sodium cacodylate at pH 6.6 buffer in the presence of 10 molar equivalents of Pep-PTN, Pep-VSE, or the DMSO solvent control. For c-MycC52, where there were two transitions, the top ΔT_M indicates the one observed at lower temperatures, and the bottom value is the second transition at higher temperatures. All data are presented as mean change in the higher Tm ± SEM (n = 4). Significance was tested with a one-way ANOVA with Bonferroni post-hoc analysis. ∗P < 0.05, ∗∗P < 0.01, ∗∗∗P < 0.001, highlighted in bold. Binding constants determined a by UV-titrations in 10 mM sodium cacodylate at pH 6.6. Values represent the average of three experiments ± standard deviation. A Kd > 50 indicates cases where evidence of binding was observed but did not plateau at the concentration range of the experiment. NS = non-specific binding indicates where no significant pattern of binding was observed at the concentration range of the experiment*

Peptide	ΔT_M (°C)					K_d (μM)				
	c-MycC27	c-MycC52	c-MycG27	c-MycG52	DS	c-MycC52	c-MycG52	DAPc	DAPg	dsDNA
PTN	0 ± 0.5; 0 ± 0.5	−1 ± 0.5; **−2 ± 0.3***	−1 ± 0.5	**+2 ± 0.3***	0 ± 0.6	0.93 ± 0.08	>50	NS	NS	NS
VSE	0 ± 0.6; −1 ± 0.6	**−3 ± 0.2**;** −14 ± 0.5***	−1 ± 0.5	**+4 ± 0.1****	0 ± 0.8	0.43 ± 0.03	>50	NS	NS	NS

iments to be performed at the highest reasonable pH possible, we also determined the binding in the presence of 100 mM KCl, and these binding affinities were also within the same ranges (Supplementary Table S6 and Supplementary Figs S11–S13). This gives about 50-fold selectivity (Pep-PTN) and 100-fold selectivity (Pep-VSE) for c-MycC52 against the complementary G4 forming sequence, or indeed any other DNA structure examined. Despite the demonstrable importance of the extended five-tract C-rich sequence within the c-Myc promoter [30], most studies looking at ligand binding use the shorter sequences. Some examples include Dash and coworkers, who demonstrated ligands PBP1 and PBP2 that could bind the short c-Myc sequence with K_ds of 2.4 and 9.5 μM, respectively [48] and that a triazole containing ligand (3be) has an apparent K_d value of 0.25 μM [47]. Mitoxantrone and analogues showed a range of K_d values for these ligands against the short c-Myc iM-forming sequence between 6.8 and 38 μM [50], and tobramycin was also found to bind c-Myc with a K_d of 13 μM [35]. Analogues of bisacridines have reported binding affinities of between 1 and 26 μM [51], and acridone derivatives show binding between 4.6 and 6.8 μM [52]. The K_d values for these peptides against c-MycC52 (PTN = 0.93 ± 0.08 μM and VSE = 0.43 ± 0.03 μM) are lower than those of all but one of the reported ligands binding to c-Myc. The iM-specific antibody has un-matched affinity for the c-Myc iM structure (K_d = 409 pM), but data are reported only for binding to the shorter c-Myc sequence. Although the iM-targeting antibody is specific for iM as a structure, it also binds multiple types of iM-structures [24, 53]. Here, these peptides demonstrate unprecedented specificity for the iM from c-Myc under the examined conditions.

The profound iM-interacting capabilities of these peptides prompted us to examine if they could modulate gene expression in cells. The widely used Del-4 c-Myc promoter reporter construct was selected to investigate the biological effects of the peptide delivery into cells. The large molecular mass (>1500 g/mole) of the peptides prompted us to use Nanocin Pro® to enhance cellular uptake. Relative c-Myc promoter activity was measured in a dual reporter gene assay by normalizing Firefly expression, which is proportional to c-Myc expression, and *Renilla* luciferase expression as an internal control (Fig. 2A). Treatment with 10 μM Pep-PTN and Pep-VSE caused concentration-dependent decreases in luciferase activity of ($P < 0.001$) compared to the vehicle-only control (Nanocin Pro® + 0.2% DMSO). This indicated that the peptides cause a decrease in c-Myc promoter activity. This is in-line with the hypothesis proposed by Hurley *et al.* in their study of the C-rich sequences from the promoter region of Bcl-2 [54]. In their study, they showed that stabilization of iM structure resulted in an increase in expression of Bcl-2. Our peptides have the opposite biophysical properties and the opposite biological effects. Experiments conducted without the Nanocin Pro® delivery agent also showed that the peptides retained their activity, although the effect was reduced compared to treatments that included Nanocin Pro®. (Supplementary Fig. S14). We were not only interested in understanding the specificity of the effects on c-Myc promoter activity but also examined the effects of the peptides against an analogous reporter gene from the insulin promoter, which contains the iM-forming sequence from the ILPR [38]. In contrast to the reduction in promoter activity for the c-Myc promoter in the presence of the peptides, there was no significant change in response in the insulin promoter (Fig. 2A), demonstrating that Pep-VSE and Pep-PTN have some specificity for the iM from c-Myc.

Cell proliferation assays were conducted concurrently with the luciferase assays (Fig. 2B). The peptides had no significant effect on proliferation in HEK293 wild-type cells (Fig. 2B and Supplementary Fig. S15A). To examine whether there were any potential effects on cells which could have arisen from the reduction in c-Myc expression, we determined the effects on cell proliferation in MCF-7 and PANC-1 cells, examples of cell lines in which proliferation is driven by c-Myc [55, 56]. Both MCF-7 and PANC-1 cells showed significant, time-dependent reduction in cell proliferation after addition of the peptides, in-line with an effect of suppressing c-Myc transcription firing on a background of high Myc-driven cell proliferation (Supplementary Fig. S16). Interestingly, we observed that HEK293 cells transfected with the c-Myc reporter gene demonstrated reduced proliferation in the presence of the peptides compared to untransfected controls (Fig. 2B). Whereas the peptides did not affect proliferation significantly in cells transfected with the ILPR reporter gene (Supplementary Fig. S15B). This is indicative of the diversion of the cellular machinery to the c-Myc reporter gene in HEK293 cells when exposed to the peptides.

Given the selectivity of the Pep-PTN and Pep-VSE peptides for the c-Myc iM structure, both in the binding experiments and also the *in vitro* gene assays, we considered potential binding modes. We recorded NMR spectra of the c-MycC52 oligonucleotide in the presence and absence of Pep-VSE to give insights into potential binding sites (Supplementary Figs S17–S20). In the presence of one equivalent of Pep-VSE, we

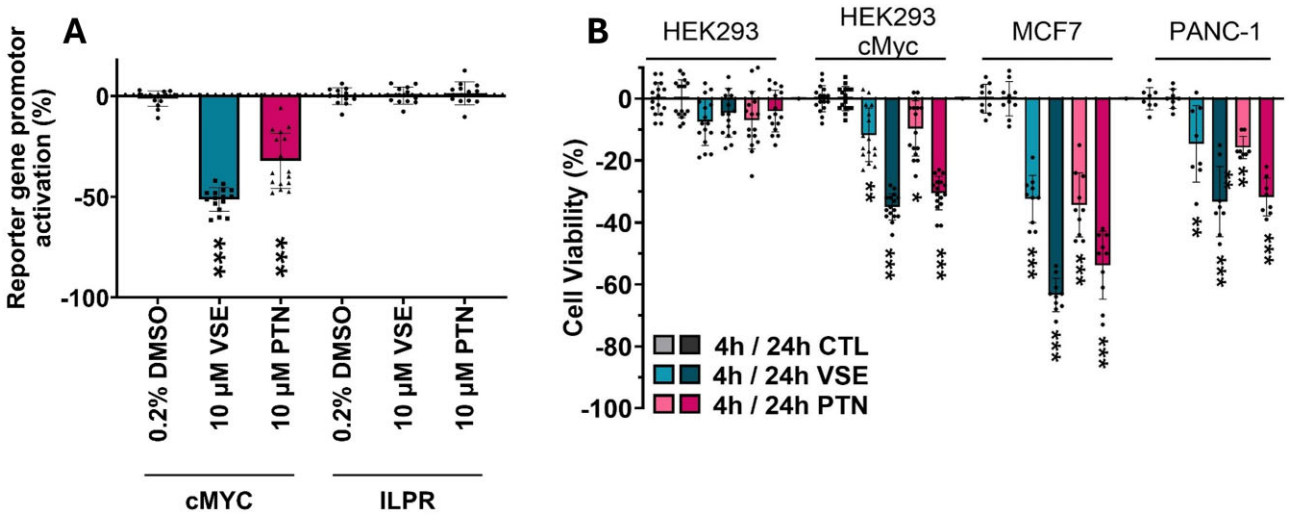

Figure 2. A) Difference in reporter gene activation in HEK293 cells transfected with c-Myc or ILPR after 4 h of treatment in the presence of Nanocin Pro® (+) with peptide VSE or PTN at 10 μM. The scattered plots represent eight biological repeats for HEK293(+c-Myc-reporter) and six biological repeats for HEK293(+ILPR-reporter), each with two technical repeats. Data shown are mean ± SD ($n = 5/6$), ***$P < 0.001$ determined by a one-way ANOVA with Holm–Šídák post-hoc analysis. (**B**) Relative change in cell viability of HEK293, HEK293(+c-Myc-reporter), MCF-7, and PANC-1 cells after 4 and 24 h of treatment in the presence of Nanocin Pro® (+) with peptide VSE or PTN at 10 μM. Control (CTL) is treated the same except without peptide (media with DMSO at the same concentration/volume as the treatments). The scattered plots represent six biological repeats for MCF-7 and five biological repeats for HEK293–ILPR, each with two technical repeats. Data shown are mean ± SD ($n = 5/6$), *P < 0.05, $P < 0.01$, $P < 0.001$ determined by a one-way ANOVA with Holm–Šídák post-hoc analysis.

observe no perturbations to imino resonances, indicating that the DNA remains structured in the presence of the peptide; we also observe that the peptide is soluble and not aggregated and the pH does not shift upon titration. The peptide spectra show some chemical shift changes in aromatic resonances (7–8 ppm, Supplementary Figs S19 and S20), which based on chemical shift and multiplicity, are likely to arise from the tryptophan residues. The changes in signal are small, which indicates either that binding occurs in the loops far from base pairs; hence, we see no perturbation in these signals upon binding, or the peptide remains in a disordered conformation upon binding, so that chemical shifts are not perturbed far from their ensemble-averaged values upon binding. Given the specificity, binding, and stabilization experiments indicating strong interactions between Pep-VSE and c-Myc, this is then consistent with a model where the peptide binds the loops, and not the core C-stack or grooves. The absence of structural information on the long c-Myc iM-forming sequence led us to create models based on the existing intramolecular iM structure from the ILPR [38], and the previous folding conformations proposed by Sutherland *et al.* [30] (see Supplementary Information). Molecular dynamic simulations were employed (Supplementary Figs S22 and S23), and subsequently docking was performed to explore interactions between the peptides and two distinct conformations of the c-Myc iM DNA. The highest-ranked model (characterized by the most negative docking score and highest confidence score) from each docking experiment was selected as the optimal peptide–DNA complex structure (Fig. 3).

In this study, we identified several peptides which target the c-MycC52 iM sequence. Two of which we have studied in more detail to reveal their selective binding for this iM-forming sequence and their selective modulation of c-Myc transcription in intact cells. Hurley *et al.* illuminated the mutually exclusive binding of nucleolin and hnRNP-K to the c-Myc G quadruplex and iM structures, and highlighted the challenge in the design of chemical probes and drug molecules that

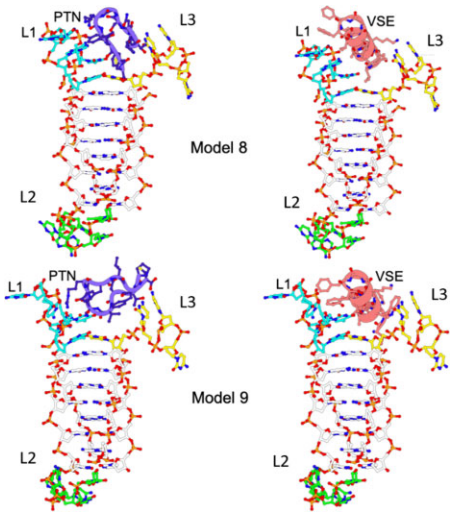

Figure 3. Models of the c-Myc iM and docked peptides Pep-PTN (purple) and Pep-VSE (salmon) between loops (L) (bases 10–14; cyan sticks) and three (bases 29–32; yellow sticks) in Model 8 (top row) and Model 9 (bottom row).

can precisely control c-Myc transcriptional firing [30]. Aberrant activation of c-Myc transcription has the potential to further promote cancer cell growth, and these peptides can serve as a counter-weight to this, either as probes on their own or in combination with other ligands. There is strong potential in using peptides to target iMs. To date, the only other peptides that have been studied to target–iM structures were targeting Hif-1-α but were not assessed for their activity [57]. The main benefit of these peptide ligands is their ease of use. Through custom commercially available peptide synthesis, there is great potential for their use as biological probes. These could be useful tools for studying c-Myc gene expression or may act as lead compounds for the development of peptidomimetic therapeutics targeting c-Myc with enhanced drug-like properties.

There are now multiple examples of successful development of small-molecule peptidomimetics [58], leaving this chemical space now open for more specific small molecules to be derived from these core peptide structures. Finally, through selecting these peptides by phage display, we also demonstrate the potential for using phage display for other iM-targets in the human genome and beyond.

Acknowledgements

We thank Dr. Nikita Harvey for supporting the NMR experiments, which were acquired using the UCL School of Pharmacy NMR Core Facility (RRID:SCR_027123).

Author contributions: Z.A.E.W. and C.J.M. secured the research funding, conceived, and designed the study. S.R. performed and analysed the Phage Display and FID experiments. D.G. designed, performed, and analysed the stabilization and binding experiments and all cell-based studies. J.K. supported D.G. with some of the preliminary reporter gene assays. E.A., S.C., and S.H. designed, performed, and analysed the computational experiments. C.A.W. performed and analysed the NMR experiments. S.R., D.G., C.J.M., and Z.A.E.W. wrote the first draft of the paper. S.R., D.G., E.A., S.H., C.A.W., C.J.M., and Z.A.E.W. contributed to the review and editing of the manuscript.

Supplementary data

Supplementary Data is available at NAR Online.

Conflict of interest

None declared.

Funding

This work was supported by the BBSRC Norwich Research Park Biosciences Doctoral Training Partnership (grant number BB/M011216/1–studentship for S.R.). D.G. was supported by the BBSRC (BB/W001616/1). Funding to pay the open access publication charges for this article was provided by the Institutional agreement.

Data availability

Data is available at 10.5281/zenodo.14258360.

References

1. Dhanasekaran R, Deutzmann A, Mahauad-Fernandez WD *et al.* The MYC oncogene—the grand orchestrator of cancer growth and immune evasion. *Nat Rev Clin Oncol* 2022;19:23–36. https://doi.org/10.1038/s41571-021-00549-2
2. Dang CV. MYC on the path to cancer. *Cell* 2012;149:22–35. https://doi.org/10.1016/j.cell.2012.03.003
3. Jain M, Arvanitis C, Chu K *et al.* Sustained loss of a neoplastic phenotype by brief inactivation of MYC. *Science* 2002;297:102–4. https://doi.org/10.1126/science.1071489
4. Jung LA, Gebhardt A, Koelmel W *et al.* OmoMYC blunts promoter invasion by oncogenic MYC to inhibit gene expression characteristic of MYC-dependent tumors. *Oncogene* 2017;36:1911–24. https://doi.org/10.1038/onc.2016.354
5. Soucek L, Whitfield JR, Sodir NM *et al.* Inhibition of Myc family proteins eradicates KRas-driven lung cancer in mice. *Genes Dev* 2013;27:504–13. https://doi.org/10.1101/gad.205542.112
6. Esain-Garcia I, Kirchner A, Melidis L *et al.* G-quadruplex DNA structure is a positive regulator of MYC transcription. *Proc Natl Acad Sci USA* 2024;121:e2320240121. https://doi.org/10.1073/pnas.2320240121
7. Rudolph C, Adam G, Simm A. Determination of copy number of c-Myc protein per cell by quantitative western blotting. *Anal Biochem* 1999;269:66–71. https://doi.org/10.1006/abio.1999.3095
8. Dani C, Blanchard JM, Piechaczyk M *et al.* Extreme instability of myc mRNA in normal and transformed human cells. *Proc Natl Acad Sci USA* 1984;81:7046–50. https://doi.org/10.1073/pnas.81.22.7046
9. Wierstra I, Alves J. The c-myc promoter: still MysterY and challenge. *Adv Cancer Res* 2008:99:113–333. https://doi.org/10.1016/S0065-230X(07)99004-1
10. Davis TL, Firulli AB, Kinniburgh AJ. Ribonucleoprotein and protein factors bind to an H-DNA-forming c-myc DNA element: possible regulators of the c-myc gene. *Proc Natl Acad Sci USA* 1989;86:9682–6. https://doi.org/10.1073/pnas.86.24.9682
11. Berberich SJ, Postel EH. PuF/NM23-H2/NDPK-B transactivates a human c-myc promoter-CAT gene via a functional nuclease hypersensitive element. *Oncogene* 1995;10:2343–7.
12. Dai J, Hatzakis E, Hurley LH *et al.* I-motif structures formed in the human c-MYC promoter are highly dynamic—insights into sequence redundancy and I-motif stability. *PLoS One* 2010;5:e11647. https://doi.org/10.1371/journal.pone.0011647
13. Gehring K, Leroy J-L, Guéron M. A tetrameric DNA structure with protonated cytosine–cytosine base pairs. *Nature* 1993;363:561–5. https://doi.org/10.1038/363561a0
14. Day HA, Pavlou P, Waller ZAE. i-Motif DNA: structure, stability and targeting with ligands. *Bioorg Med Chem* 2014;22 :4407–18. https://doi.org/10.1016/j.bmc.2014.05.047
15. Burge S, Parkinson GN, Hazel P *et al.* Quadruplex DNA: sequence, topology and structure. *Nucleic Acids Res* 2006;34:5402–15. https://doi.org/10.1093/nar/gkl655
16. Grand CL, Han H, Muñoz RM *et al.* The cationic porphyrin TMPyP4 down-regulates c-MYC and human telomerase reverse transcriptase expression and inhibits tumor growth *in vivo*. *Mol Cancer Ther* 2002;1:565–73.
17. Siddiqui-Jain A, Grand CL, Bearss DJ *et al.* Direct evidence for a G-quadruplex in a promoter region and its targeting with a small molecule to repress c-MYC transcription. *Proc Natl Acad Sci USA* 2002;99:11593–8. https://doi.org/10.1073/pnas.182256799
18. Yang D, Hurley LH. Structure of the biologically relevant G-quadruplex in the c-MYC promoter. *Nucleosides Nucleotides Nucleic Acids* 2006;25:951–68. https://doi.org/10.1080/15257770600809913
19. Brooks TA, Hurley LH. The role of supercoiling in transcriptional control of MYC and its importance in molecular therapeutics. *Nat Rev Cancer* 2009;9:849–61. https://doi.org/10.1038/nrc2733
20. Sekibo DAT, Fox KR. The effects of DNA supercoiling on G-quadruplex formation. *Nucleic Acids Res* 2017;45:12069–79. https://doi.org/10.1093/nar/gkx856
21. Brown SL, Kendrick S. The i-motif as a molecular target: more than a complementary DNA secondary structure. *Pharmaceuticals* 2021;14:96. https://doi.org/10.3390/ph14020096
22. Zhou J, Wei C, Jia G *et al.* Formation of i-motif structure at neutral and slightly alkaline pH. *Mol BioSyst* 2010;6:580–6, https://doi.org/10.1039/B919600E
23. Wright EP, Huppert JL, Waller ZAE. Identification of multiple genomic DNA sequences which form i-motif structures at neutral pH. *Nucleic Acids Res* 2017;45:2951–9. https://doi.org/10.1093/nar/gkx090
24. Zeraati M, Langley DB, Schofield P *et al.* motif DNA structures are formed in the nuclei of human cells. *Nature Chem* 2018;10:631–7. https://doi.org/10.1038/s41557-018-0046-3

25. King JJ, Irving KL, Evans CW *et al.* DNA G-quadruplex and i-motif structure formation is interdependent in human cells. *J Am Chem Soc* 2020;142:20600–4. https://doi.org/10.1021/jacs.0c11708
26. Zanin I, Ruggiero E, Nicoletto G *et al.* Genome-wide mapping of i-motifs reveals their association with transcription regulation in live human cells. *Nucleic Acids Res* 2023;51:8309–21. https://doi.org/10.1093/nar/gkad626
27. Luo X, Zhang J, Gao Y *et al.* Emerging roles of i-motif in gene expression and disease treatment. *Front Pharmacol* 2023;14:1136251. https://doi.org/10.3389/fphar.2023.1136251
28. Pagano A, Iaccarino N, Abdelhamid MAS *et al.* Common G-quadruplex binding agents found to interact with i-motif-forming DNA: unexpected multi-target-directed compounds. *Front Chem* 2018;6:281. https://doi.org/10.3389/fchem.2018.00281
29. Abdelhamid MAS, Gates AJ, Waller ZAE. Destabilization of i-motif DNA at neutral pH by G-quadruplex ligands. *Biochemistry* 2019;58:245–9. https://doi.org/10.1021/acs.biochem.8b00968
30. Sutherland C, Cui Y, Mao H *et al.* A mechanosensor mechanism controls the G-quadruplex/i-motif molecular switch in the MYC promoter NHE III(1). *J Am Chem Soc* 2016;138:14138–51. https://doi.org/10.1021/jacs.6b09196
31. Zhou W, Jie Q, Pan T *et al.* Single-cell RNA binding protein regulatory network analyses reveal oncogenic HNRNPK-MYC signalling pathway in cancer. *Commun Biol* 2023;6:82. https://doi.org/10.1038/s42003-023-04457-2
32. Qin G, Liu Z, Yang J *et al.* Targeting specific DNA G-quadruplexes with CRISPR-guided G-quadruplex-binding proteins and ligands. *Nat Cell Biol* 2024;26:1212–24. https://doi.org/10.1038/s41556-024-01448-1
33. Nuccio SP, Cadoni E, Nikoloudaki R *et al.* Individual G-quadruplex targeting with ligand-functionalized CRISPR–Cas9 uncovers transcriptional-dependent functional responses. *bioRxiv*, https://doi.org/10.1101/2024.10.14.618195, 15 October 2024, preprint: not peer reviewed.
34. Anthis NJ, Clore GM. Sequence-specific determination of protein and peptide concentrations by absorbance at 205 nm. *Protein Sci* 2013;22:851–8. https://doi.org/10.1002/pro.2253
35. Sheng Q, Neaverson JC, Mahmoud T *et al.* Identification of new DNA i-motif binding ligands through a fluorescent intercalator displacement assay. *Org Biomol Chem* 2017;15:5669–73. https://doi.org/10.1039/c7ob00710h
36. He TC Sparks AB, Rago C *et al.* Identification of c-MYC as a target of the APC pathway. *Science* 1998;281:1509–12. https://doi.org/10.1126/science.281.5382.1509
37. Kuroda A, Rauch TA, Todorov I *et al.* Insulin gene expression is regulated by DNA methylation. *PLoS One* 2009;4:e6953. https://doi.org/10.1371/journal.pone.0006953
38. Guneri D, Alexandrou E, El Omari K *et al.* Structural insights into i-motif DNA structures in sequences from the insulin-linked polymorphic region. *Nat Commun* 2024;15:7119. https://doi.org/10.1038/s41467-024-50553-0
39. Pérez A, Herrera-Nieto P, Doerr S *et al.* AdaptiveBandit: a multi-armed bandit framework for adaptive sampling in molecular simulations. *J Chem Theory Comput* 2020;16:4685–93. https://doi.org/10.1021/acs.jctc.0c00205
40. Scherer MK, Trendelkamp-Schroer B, Paul F *et al.* PyEMMA 2: a Software package for estimation, validation, and analysis of Markov models. *J Chem Theory Comput* 2015;11:5525–42. https://doi.org/10.1021/acs.jctc.5b00743
41. Liu KC, Röder K, Mayer C *et al.* Affinity-selected bicyclic peptide G-quadruplex ligands mimic a protein-like binding mechanism. *J Am Chem Soc* 2020;142:8367–73. https://doi.org/10.1021/jacs.0c01879
42. DesJardins E, Hay N. Repeated CT elements bound by zinc finger proteins control the absolute and relative activities of the two principal human c-myc promoters. *Mol Cell Biol* 1993;13:5710–24. https://doi.org/10.1128/mcb.13.9.5710-5724.1993
43. Sloth AB Bakhshinejad B, Jensen M *et al.* Analysis of Compositional Bias in a Commercial Phage Display Peptide Library by Next-Generation Sequencing. *Viruses* 2022;14:2402. https://doi.org/10.3390/v14112402
44. Dexheimer TS, Carey SS, Zuohe S *et al.* NM23-H2 may play an indirect role in transcriptional activation of c-myc gene expression but does not cleave the nuclease hypersensitive element III(1). *Mol Cancer Ther* 2009;8:1363–77. https://doi.org/10.1158/1535-7163.MCT-08-1093
45. Mergny J-L, Lacroix L, Han X *et al.* Intramolecular folding of pyrimidine oligodeoxynucleotides into an i-DNA motif. *J Am Chem Soc* 1995;117:8887–98. https://doi.org/10.1021/ja00140a001
46. Shu B, Cao J, Kuang G *et al.* Syntheses and evaluation of new acridone derivatives for selective binding of oncogene c-myc promoter i-motifs in gene transcriptional regulation. *Chem Commun* 2018;54:2036–9. https://doi.org/10.1039/C8CC00328A
47. Saha P, Panda D, Müller D *et al. In situ* formation of transcriptional modulators using non-canonical DNA i-motifs. *Chem Sci* 2020;11:2058–67, https://doi.org/10.1039/D0SC00514B
48. Debnath M, Ghosh S, Chauhan A *et al.* Preferential targeting of i-motifs and G-quadruplexes by small molecules. *Chem Sci* 2017;8:7448–56. https://doi.org/10.1039/C7SC02693E
49. Di Porzio A, Galli U, Amato J *et al.* Synthesis and characterization of bis-triazolyl-pyridine derivatives as noncanonical DNA-interacting compounds. *Int J Mol Sci* 2021;22:11959. https://doi.org/10.3390/ijms222111959
50. Wright EP, Day HA, Ibrahim AM *et al.* Mitoxantrone and analogues bind and stabilize i-motif forming DNA sequences. *Sci Rep* 2016;6:39456. https://doi.org/10.1038/srep39456
51. Kuang G, Zhang M, Kang S *et al.* Syntheses and evaluation of new bisacridine derivatives for dual binding of G-quadruplex and i-motif in regulating oncogene c-myc expression. *J Med Chem* 2020;63:9136–53. https://doi.org/10.1021/acs.jmedchem.9b01917
52. Shu B, Cao J, Kuang G *et al.* Syntheses and evaluation of new acridone derivatives for selective binding of oncogene c-myc promoter i-motifs in gene transcriptional regulation. *Chem Commun* 2018;54:2036–9. https://doi.org/10.1039/c8cc00328a
53. Ruggiero E, Marusic M, Zanin I *et al.* The iMab antibody selectively binds to intramolecular and intermolecular i-motif structures. *Nucleic Acids Res* 2025;53. https://doi.org/10.1093/nar/gkae1305
54. Kendrick S, Kang HJ, Alam MP *et al.* The dynamic character of the BCL2 promoter i-motif provides a mechanism for modulation of gene expression by compounds that bind selectively to the alternative DNA hairpin structure. *J Am Chem Soc* 2014;136:4161–71. https://doi.org/10.1021/ja410934b
55. Buchholz M, Schatz A, Wagner M *et al.* Overexpression of c-myc in pancreatic cancer caused by ectopic activation of NFATc1 and the Ca^{2+}/calcineurin signaling pathway. *EMBO J* 2006;25:3714–24. https://doi.org/10.1038/sj.emboj.7601246
56. Wang YH, Liu S, Zhang G *et al.* Knockdown of c-Myc expression by RNAi inhibits MCF-7 breast tumor cells growth in vitro and in vivo. *Breast Cancer Res* 2005;7:R220–228. https://doi.org/10.1186/bcr975
57. Ghosh D, Pratihar S, Govindaraju T. Designer tryptophan-rich peptide modulates structural dynamics of HIF-1α DNA i-motif DNA. *J Pept Sci* 2024;30:e3601. https://doi.org/10.1002/psc.3601
58. Li Petri G, Di Martino S, De Rosa M. Peptidomimetics: an overview of recent medicinal chemistry efforts toward the discovery of novel small molecule inhibitors. *J Med Chem* 2022;65:7438–75. https://doi.org/10.1021/acs.jmedchem.2c00123

Received: December 5, 2024. **Revised:** September 22, 2025. **Accepted:** September 23, 2025